Journal of Experimental Botany, Vol. 71, No. 21 pp. 6830–6843, 2020
doi:10.1093/jxb/eraa258 Advance Access Publication 2 June 2020

RESEARCH PAPER

Siliplant1 protein precipitates silica in sorghum silica cells

Santosh Kumar[1,*,†], Nurit Adiram-Filiba[2], Shula Blum[1], Javier Arturo Sanchez-Lopez[3], Oren Tzfadia[4], Ayelet Omid[5], Hanne Volpin[5], Yael Heifetz[3], Gil Goobes[2] and Rivka Elbaum[1,*]

[1] Robert H Smith Institute of Plant Sciences and Genetics in Agriculture, Robert H Smith Faculty of Agriculture, Food and Environment, Hebrew University of Jerusalem, Rehovot 7610001, Israel
[2] Department of Chemistry, Bar-Ilan University, Ramat Gan 5290002, Israel
[3] Department of Entomology, Robert H Smith Faculty of Agriculture, Food and Environment, Hebrew University of Jerusalem, Rehovot 7610001, Israel
[4] Bioinformatics and Systems Biology, VIB/Ghent University, Gent B-9052, Belgium
[5] Danziger Innovations Limited, Mishmar Hashiva 5029700, Israel

[†] Present address: Electron Microscopy Facility, Centre for Cellular and Molecular Platforms (C-CAMP), National Centre for Biological Sciences (NCBS-TIFR), Bangalore 560065, India.
* Correspondence: skg.research@gmail.com or rivka.elbaum@mail.huji.ac.il

Received 8 January 2020; Editorial decision 14 May 2020; Accepted 26 May 2020

Editor: Marek Vaculik, Comenius University in Bratislava, Slovakia

Abstract

Silicon is absorbed by plant roots as silicic acid. The acid moves with the transpiration stream to the shoot, and mineralizes as silica. In grasses, leaf epidermal cells called silica cells deposit silica in most of their volume using an unknown biological factor. Using bioinformatics tools, we identified a previously uncharacterized protein in *Sorghum bicolor*, which we named Siliplant1 (Slp1). Slp1 is a basic protein with seven repeat units rich in proline, lysine, and glutamic acid. We found *Slp1* RNA in sorghum immature leaf and immature inflorescence. In leaves, transcription was highest just before the active silicification zone (ASZ). There, Slp1 was localized specifically to developing silica cells, packed inside vesicles and scattered throughout the cytoplasm or near the cell boundary. These vesicles fused with the membrane, releasing their content in the apoplastic space. A short peptide that is repeated five times in Slp1 precipitated silica *in vitro* at a biologically relevant silicic acid concentration. Transient overexpression of Slp1 in sorghum resulted in ectopic silica deposition in all leaf epidermal cell types. Our results show that Slp1 precipitates silica in sorghum silica cells.

Keywords: Biomineralization, phytolith, silica cell, silicification, Siliplant1 (Slp1), *Sorghum bicolor*.

Introduction

Grasses are well known for their high silica ($SiO_2 \cdot nH_2O$) content, reaching up to 10% of their dry weight (Hodson *et al.*, 2005). Silicon is available to plants as mono-silicic acid [$Si(OH)_4$] whose concentration in soil solution usually varies between 0.1 mM and 0.6 mM (Epstein, 1994). Grass roots actively take up silicic acid from soil (Ma *et al.*, 2006, 2007) of which ≥90% is loaded into the xylem (Yoshida *et al.*, 1962). A cooperative uptake of silicic acid by two root transporters leads to Si supersaturation in the grass xylem sap (Sakurai *et al.*, 2015). The Si concentration may reach 5–7.5 mM, which is 3–4 times higher than its saturation concentration (Ma *et al.*, 2002; Casey *et al.*, 2003; Mitani and Ma, 2005). Silicic acid

Abbreviations: ASZ, active silicification zone; MAS, magic angle spinning; Slp1, Siliplant1; ss-NMR, solid-state NMR.

molecules then move with the transpiration stream inside the plant body to reach the shoots, where they are unloaded from the xylem (Yamaji *et al.*, 2008). Finally, silicic acid polymerizes as solid biogenic silica at several locations inside the plant body. The most prominent deposition of silica in grasses is impregnation of cell walls of leaf epidermal cells, abaxial epidermal cells of the inflorescence bracts (glumes and lemma), and root endodermal cells. The silicification mechanism across the cell types is not uniform (Zancajo *et al.*, 2019). Models of deposition suggest either spontaneous formation as a result of evapo-transpirational loss of water, or a tightly controlled process (Kumar *et al.*, 2017*b*). Uptake of silicic acid and its deposition are also affected by mechanically damaging the plant (McLarnon *et al.*, 2017), and possibly other unknown physiological factors affecting root silicon transporters (Talukdar *et al.*, 2019).

Silica cells are one of the cell types most frequently silicified in grass leaves (Motomura *et al.*, 2000; Kumar and Elbaum, 2018). Silica cells are specialized epidermal cells occurring mostly as silica–cork cell pairs, both above and below the leaf longitudinal veins (Kaufman *et al.*, 1985), on internode epidermis (Kaufman *et al.*, 1969), and on the abaxial epidermis of glumes (Hodson *et al.*, 1985). We earlier estimated that the whole process of leaf silica cell silicification is completed within 10 h of cell division (Kumar and Elbaum, 2018). Within this time period, almost the entire cell lumen is filled with solid silica (Hodson *et al.*, 1985). Silica cell silicification is immediately followed by cell death (Kumar and Elbaum, 2018) which terminates the silicification process (Kumar *et al.*, 2017*a*; Kumar and Elbaum, 2018; Markovich *et al.*, 2019). Silicification in silica cells is different from that in other studied systems. In lemma epidermal cells (e.g. macro-hairs and long cells), silica deposits during the course of weeks on the thickened cell wall material (Hodson *et al.*, 1984; Perry *et al.*, 1984); in glume prickle hairs and papillae, silica is deposited in the empty lumen of these cells even after cell death (Hodson *et al.*, 1985); and, on the thickened inner tangential cell wall of root endodermal cells, modified lignin residues nucleate silica (Zexer and Elbaum, 2020). Plant silica was suggested to be templated on cell wall polymers such as mixed-linkage glucan (Fry *et al.*, 2008), callose (Law and Exley, 2011; Brugiére and Exley, 2017; Kulich *et al.*, 2018), and modified lignin (Zhang *et al.*, 2013; Soukup *et al.*, 2017, 2020; Zexer and Elbaum, 2020). The template of lumen silicification in silica cells is currently unknown. Interestingly, silica in wheat (*Triticum durum*) silica cells has continuously distributed occluded organic matter. The N/C ratio suggests the presence of amino acids in the silica (Alexandre *et al.*, 2015). Several proteins are associated with bio-silica in unicellular and multicellular organisms (Perry, 2003); for example, silaffins (Kröger *et al.*, 1999; Poulsen and Kröger, 2004), silacidins (Wenzl *et al.*, 2008), and silicanin-1 (Kotzsch *et al.*, 2017) from diatoms, and silicateins (Shimizu *et al.*, 1998) and glassin (Shimizu *et al.*, 2015) from sponges. Among plants, a short peptide derived from an inducible proline-rich protein precipitates silica *in vitro*. The protein, involved in systemic acquired resistance in cucumber, may precipitate silica locally at attempted fungal penetration sites (Kauss *et al.*, 2003). The above-mentioned protein groups do not share sequence homology.

We study silica deposition in silica cells of sorghum (*Sorghum bicolor*), a member of the grass (Poaceae) family. Sorghum is categorized as an active silica accumulator (Hodson *et al.*, 2005; Coskun *et al.*, 2019*a*). In grasses there is a very simple and clear gradient of cell maturation along the long axis of leaves: the leaf epidermal cell division zone is confined to the base of the leaf and the newly divided cells displace the maturing cells away from the leaf base. Hence, leaf epidermal cells that are close to the leaf apex are older than the cells close to the base (Skinner and Nelson, 1995).

Silica cell silicification is confined to elongating leaves, in a well-defined active silicification zone (ASZ). The ASZ itself resides in the middle of the leaf, between 40% and 60% of the leaf length (Kumar *et al.*, 2017*a*; Kumar and Elbaum, 2018). The mineralization initiates in the apoplastic space of viable silica cells, producing a thick silica wall that confines the cytoplasmic space to smaller and smaller volumes (Kumar *et al.*, 2017*a*; Kumar and Elbaum, 2018). During this fast process, the cell maintains cell–cell connectivity to the neighbouring cells through plasmodesmata (Kumar *et al.*, 2017*a*). As the silicic acid is available in the apoplast in supersaturation, a crucial stage would be the initiation of controlled silica deposition. A possible way could be by adding to the cell wall a biomineralizing protein at an appropriate time and place. Here, we report on a previously uncharacterized protein that is expressed in silica cells and exported to the cell wall during their silicification. This protein induces precipitation of silica *in vivo*. Hence, we named this protein Siliplant1 (Slp1).

Materials and methods

Plant material, growth conditions, and tissue nomenclature

Caryopses of *Sorghum bicolor* (L.) Moench (line BTx623) were surface sterilized and germinated in soil as reported previously (Kumar and Elbaum, 2018). Unless indicated otherwise, we analysed sorghum seedlings of ~2 weeks of age. Immature, silicifying leaf (L_{IS}) in this study is analogous to leaf-2, as reported in our earlier studies (Kumar and Elbaum, 2017, 2018; Kumar *et al.*, 2017*a*). The immature leaf was cut into five equal segments. The middle segment is most active in terms of silica cell silicification (Kumar *et al.*, 2017*a*; Kumar and Elbaum, 2018) and was named the ASZ. The segment just older than the ASZ (towards the leaf tip, represented by between 60% and 80% of the leaf length) was named ASZ+1, while the segment just younger than ASZ (towards the leaf base, represented by between 20% and 40% of the leaf length) was named ASZ–1. The youngest segment (at the leaf base, up to 20% of the leaf length) was named ASZ–2. Mature leaves were cut into 10 equal segments and only the eighth segment from the leaf base (between 70% and 80% of the leaf length) was used for all the experiments.

Screening for putative silicification protein(s)

Candidate silicification proteins were searched in a publicly available data set which reports the influence of silicon treatments on gene expression in wheat (GEO NCBI dataset GSE12936) (Chain *et al.*, 2009). Genes that are co-expressed with wheat silicon transporter genes (*TaLsi1*, *TaLsi2*, and *TaLsi6*), irrespective of the plant pathogenic infection status, were identified using the Comparative Co-Expression Network Construction and Visualization (CoExpNetViz) online tool (Tzfadia *et al.*, 2015). The probe sequences of the candidate wheat genes were extracted and used to BLAST against the sorghum genome. We identified 18 sorghum

orthologue genes (an e-value >e^{-100} was used as the orthology cut-off) (see Supplementary Table S1 at *JXB* online). The primary sequences of all the initially screened proteins were analysed for the theoretical isoelectric point (pI) using the ProtParam tool in the ExPASy server (https://web.expasy.org/protparam/), and for the presence of predicted signal peptide (SignalP server). Since positively charged amino acids have been shown to be involved in biological silicification, we discarded all the proteins with a predicted pI value <7. We also rejected the proteins that lacked a predictable signal peptide, needed for a protein to be secreted and induce silicification in the apoplastic space, in agreement with our previously proposed mechanism (Kumar *et al*., 2017*a*).

Sequence-based analyses of Slp1

Secondary structure was predicted by GOR4 (Combet *et al*., 2000). Intrinsically disordered tertiary structure was predicted using IUPred, under 'long disorder' type (Dosztányi *et al*., 2005*a*, *b*). Residues with a score >0.5 were regarded as disordered. SignalP was used to predict the signal peptide in Slp1 (Petersen *et al*., 2011). TargetP was used to predict whether the protein is secretory in nature (Emanuelsson *et al*., 2000). The organism group selected was 'plant', and the program was run with default cut-off selection.

Silica precipitation in vitro

Slp1 was produced in *Escherichia coli* transformed with a pET-28a(+) vector containing *Slp1* cDNA amplified by the primers Slp1-Infusion-F and Slp1-Infusion-R (see Supplementary Table S2). After expression, the protein was concentrated on a nickel-NTA column (PureCube Ni-NTA Agarose, Cube Biotech, Monheim Germany) in phosphate buffer at pH 7.0, following the procedure of Kaleda *et al*. (2019). We purchased Peptide-1: HKKPVPPKPKPEPK, a sequence that appears five times in the Slp1 primary sequence and Peptide-3: HAAPVPPAPAPEPA, where all lysine groups in Peptide-1 were replaced by alanine [GL Biochem (Shanghai) Ltd., Shanghai, China].

We prepared a fresh stock solution of 1 M silicic acid by mixing tetramethyl orthosilicate and 1 mM HCl in a volumetric ratio of 3:17 for 4 min under gentle stirring. Precipitation experiments were conducted in 1.5 ml Eppendorf tubes, except for large-scale precipitation experiments needed for NMR analysis that were conducted in 50 ml falcon tubes. Precipitation using full-length Slp1 (lacking the signal peptide) was conducted in a 90.9 mM silicic acid solution and 10–20 mg ml^{-1} protein in 0.1 M potassium phosphate buffer, pH 7.0, incubated for 5 min, and then centrifuged for 30 min. As a negative control, we extracted the proteins of bacteria expressing the vector without Slp1. Precipitation using synthetic peptides was conducted by incubating 50 µl of peptide solution (1.5 or 2.0 mg ml^{-1} in 0.1 M potassium phosphate buffer, pH 7.0) with 5 µl of 1 M silicic acid (final silicic acid concentration of 90.9 mM) for 5 min under gentle shaking at room temperature. Precipitation at physiological silicic acid concentration in grass sap (at least 5 mM) was conducted by incubating 100 µl of Peptide-1 solution (1.5 mg ml^{-1} in 0.1 M potassium phosphate buffer, pH 7.0) with 10 µl of 55 mM silicic acid (final concentration of 5 mM) for 30 min under gentle shaking. For large-scale silica precipitation of ~100 mg, we incubated 30 mg of the peptide (1.5 mg ml^{-1} in 0.1 M potassium phosphate buffer, pH 7.0) with 2 ml of 1 M silicic acid solution (final concentration of 90.9 mM) for 30 min at room temperature under gentle shaking. Sediment was collected by centrifugation at 14 000 *g* for 5 min, except for large-scale precipitation, where the sediment was collected by centrifugation at 5000 *g* for 5 min (Peptide-1) or 20 min (Peptide-3). The supernatant was discarded, and the pellet was washed three times with deionized water. For all the peptide–silica precipitation experiments, the same reactions lacking any peptide served as control. The precipitates were left to dry under ambient conditions or dried at 60 °C.

Raman spectroscopy

Lyophilized peptide solution was reconstituted in double-distilled water (50 mg ml^{-1}) and 1 µl of this solution was put on a steel slide and dried at 37 °C for 30 min before measurement. Dried powder of silica precipitate with 90.9 mM silicic acid was mounted on a steel slide. Raman spectra of the samples were collected using an InVia microspectrometer (Renishaw, New Mills, UK) equipped with a polarized 532 nm laser (45 mW maximum intensity, 4 μm^2 beam) excitation under a ×50 air objective lens (Peptide-1 and Peptide-3) and water immersion ×63 objective (Slp1). Spectra were analysed in WiRE3 (Renishaw), including smoothing, background subtraction, normalization, and peak picking.

Solid-state NMR spectroscopy

Solid-state NMR spectra were recorded on a Bruker 11.7 T Avance III spectrometer (Billerica, MS, USA) equipped with a 4 mm VTN CPMAS probe at a spinning rate of 10 kHz. The ^{29}Si cross-polarization experiment was done with 8192 scans and a recycle delay of 6 s, and the ^{29}Si direct excitation experiment was recorded with 2560 scans and a recycle delay of 60 s. Analysis of the ^{29}Si spectrum was done using the DMFIT program (Massiot *et al*., 2002). ^{13}C cross-polarization was done with 2048 scans using a recycle delay of 5 s.

Tissue-specific expression of Slp1 in sorghum

Polyclonal antibodies against Peptide-1 were raised in rabbit and purified using an antigen affinity column (GenScript, NJ, USA). Crude proteins from root tissues, the whole of immature silicifying leaves, mature leaves, and immature inflorescence (expected to emerge from the flag leaf of mature plants within a week) were extracted using a phosphate buffer [0.1 M potassium phosphate buffer, pH 7.0; 1% protease inhibitor cocktail (Sigma, St. Louis, MO, USA); and 0.1% 2-mercaptoethanol (Sigma)]. A 48 µg aliquot of the extracted protein from each sample was loaded in separate wells and run on a 15% polyacrylamide separating gel under denaturing conditions. The gel was blotted onto a nitrocellulose membrane and blocked with 5% milk powder in Tris-buffered saline (pH 7.6) containing 0.1% Tween-20 for 1 h. We incubated the membrane with purified polyclonal antibody against Peptide-1 (1 µg ml^{-1}) at 4 °C overnight. The membrane was washed and incubated with secondary antibody (anti-rabbit IgG mouse monoclonal antibody, Genscript, NJ, USA) conjugated with horseradish peroxidase. Chemiluminescence was developed (PerkinElmer, Akron, OH, USA) and the membrane was scanned for 1 s using ImageQuant LAS 4000 mini (GE Healthcare, Chicago, IL, USA) scanner.

Transcript abundance of Slp1

Transcription of *Slp1* was estimated in immature leaf, mature leaf, and immature inflorescence. RNA was isolated and cDNA was synthesized from 1 µg of total RNA after on-column DNase treatment (Zymoresearch, CA, USA). An equal volume of cDNA was PCR amplified using the primers specific for *Slp1* (Slp1-RT-F and Slp1-RT-R, Supplementary Table S2) and ubiquitin-conjugating enzyme (UbCE; Sb09g023560, UbCE-RT-F and UbCE-RT-R, Supplementary Table S2) as the reference gene (Shakoor *et al*., 2014; Markovich *et al*., 2019).

Relative transcript abundance of *Slp1* was measured in ASZ–2, ASZ–1, ASZ, ASZ+1, and the youngest mature leaf, following recommendations of Bustin *et al*. (2009) for plant tissues. Three sorghum seedlings with immature leaf length between 13 cm and 16 cm were used. RNA isolation and cDNA synthesis were carried out as described above. Reactions were performed using SYBR mix (Invitrogen, Waltham, MA, USA) in a 7300 Real Time PCR machine (Applied Biosystems, Waltham, MA, USA) following Markovich *et al*. (2019), except that the primer concentrations were kept at 150 nM each. A melt curve analysis at the end of the PCR cycle was carried out to ensure that only one PCR product was formed. *Slp1* and *UbCE* transcripts were amplified (Supplementary Table S2). In addition, we also amplified transcripts of an RNA recognition motif-containing protein (*RRM*; Sb07g027950) as another reference gene (Shakoor *et al*., 2014) using the primers RRM-RT-F and RRM-RT-R (Supplementary Table S2).

Using *UbCE* as reference gene, the relative transcript abundance of *Slp1* was calculated according to the formula of Pfaffl (2001). The relative transcript level of *RRM* is also reported, showing that the transcript levels of the two reference genes do not change significantly in the tested tissues (Supplementary Fig. S1). For statistical analysis, we used the Student's *t*-test ($P \leq 0.05$) of the program Microsoft Excel.

Immunolocalization of Slp1 in sorghum leaves

Leaf tissues from the ASZ and mature leaves were cut into pieces of ~1×1 mm^2 and fixed in 4% para-formaldehyde (w/v) and 0.05% Triton X-100, by vacuum infiltration. Blocking was done in phosphate-buffereed saline (PBS) containing 0.1% BSA. Samples were incubated with purified polyclonal antibody against Peptide-1 (10 μg ml^{-1}) for 1 h at room temperature. After washing, the samples were incubated with secondary antibody (goat anti-rabbit IgG) tagged with Alexa fluor 488, and further washed and incubated for 10 min in propidium iodide (5 μg ml^{-1}) solution. Samples underwent the same treatment (i) with pre-immune serum or (ii) without the primary or the secondary antibodies; or (iii) without both the antibodies used as control. The samples were mounted on a microscope slide and observed under a Leica SP8 inverted confocal laser scanning microscope (CLSM) with a solid-state laser (Wetzlar, Germany). Alexa fluor 488 was excited at 488 nm, and emission was collected at 500–550 nm. Propidium iodide was excited at 514 nm, and emission was collected at 598–634 nm.

Transient overexpression of Slp1 in tobacco (Nicotiana benthamiana Domin)

The pBIN-19 plasmid was modified by inserting the *Cauliflower mosaic virus* (CaMV) 35S promoter between the *Hin*dIII and *Sal*I restriction sites, and green fluorescent protein (GFP) followed by a *nos* terminator between the *Xba*I and *Eco*RI restriction sites. The resulting plasmid (pBIN-GFP) was used as control plasmid to drive the expression of GFP under the control of the CaMV 35S promoter. Primers Slp1-SalI-F and Slp1-XbaI-R (Supplementary Table S1) were used to amplify the full length of Slp1 without the stop codon and flanked with the restriction sites *Sal*I and *Xba*I, respectively. The PCR product was digested with *Sal*I and *Xba*I, and ligated to the *Sal*I- and *Xba*I-digested pBIN-GFP plasmid. The expression cassette consisted of CaMV 35S promoter–Slp1–GFP–*nos* terminator. We transformed the plasmids into *Agrobacterium tumefaciens* (strain EHA105) and infiltrated *N. benthamiana* source leaves on the abaxial side with slight modifications from the reported protocol (Li, 2011). Our resuspension solution consisted of 50 mM MES buffer and 2 mM NaH_2PO_4 supplemented with 200 μM acetosyringone (Sigma). After 48 h, leaf pieces were observed under a CLSM (excitation, 488 nm; emission filter range, 500–550 nm).

Transient overexpression of Slp1 in sorghum

We created a construct exploiting the *Maize dwarf mosaic virus* (MDMV) genome (https://patentscope.wipo.int/search/en/detail.jsf?docId=WO2016125143). We fused the expression cassette containing the CaMV 35S promoter driving the expression of Slp1 and the *nos* terminator in between *Age*I and *Apa*I restriction sites to the MDMV genome as follows. We amplified the full length of Slp1 except the start and stop codons using the primers Slp1-AgeI-F and Slp1-ApaI-R (Supplementary Table S2). After digestion of the PCR product with *Age*I and *Apa*I restriction enzymes, we ligated the digested PCR product with *Age*I- and *Apa*I-digested MDMV-GUS (β-glucuronidase) plasmid. The resulting plasmid was named MDMV-Slp1. The plasmids were coated on gold microparticles (1 μm diameter, Bio-Rad, Hercules, CA, USA) and bombarded on ~1-week-old sorghum seedlings according to the protocol of Jose-Estanyol (2013) with the following modifications. Sorghum seeds were surface sterilized, germinated, and then grown with their roots immersed in tap water for up to 7 d before they were bombarded. Just before bombardment, the seedling roots were quickly taken out of water, and a bunch of five seedlings were arranged and loosely stuck in the centre of a Petri dish and bombarded with the plasmid-coated gold particles using 1100 psi rupture discs. After bombardment, the seedlings roots were wrapped in moist tissue paper and put in a beaker with tap water for 24 h, following which the bombarded seedlings were transferred to soil. The seedlings were grown for ~3 weeks and the phenotypes in the leaves showing viral symptoms were observed by SEM. RNA was isolated from the young leaves of the infected plants and cDNA was synthesized. Slp1 with viral flanking regions was amplified by PCR with the primers MDMV-Slp1-F and MDMV-Slp1-R (Supplementary Table S1). Viral protein coat was amplified by PCR with the primers MDMV-Coat-F and MDMV-Coat-R (Supplementary Table S1) to ascertain the viral infection in the control plants infected by MDMV-GUS plasmid. We conducted this experiment twice, each time starting with 15 independent biological replicates and analysing altogether 10 plants showing strong viral symptoms.

SEM and energy dispersive X-ray spectroscopy (EDS)

Images were collected in a Jeol JSM IT100 (Peabody, MA, USA) scanning electron microscope equipped with an inbuilt EDS detector. Pellets resulting from Slp1–silicic acid and peptide–silicic acid interaction were resuspended in deionized water and smeared on carbon tape, air dried, and coated with iridium for SEM imaging in high vacuum mode using a secondary electron detector (SED). Leaf tissues were cut into small pieces (~5 mm×5 mm), stuck on carbon tape, and observed without any coating in low vacuum mode (50–70 Pa) using a back-scattered electron (BSE) detector. The beam energy was 20 keV, the probe current was 70 nA, and the working distance was between 10 mm and 11 mm. EDS maps were acquired for at least 5 min.

Results

Molecular architecture of sorghum Slp1 is similar to that of other silica-precipitating proteins

Based on our selection criteria (see above), we identified a candidate protein in sorghum (Sb01g025970), which we later named Siliplant1 (Slp1). Slp1 has seven repeat units rich in lysine, similar to silaffins from *Cylindrotheca fusiformis*, a diatom species (Kröger *et al.*, 1999); histidine–aspartic acid-rich regions similar to glassin from a marine sponge, *Euplectella* (Shimizu *et al.*, 2015); and several proline residues as in a proline-rich protein (PRP1) from cucumber (Kauss *et al.*, 2003). The alignment of nucleotide sequences of Slp1 and its corresponding wheat (*Triticum aestivum*) locus identifier Ta#S18008495 is given in Supplementary Fig. S2. Sorghum Slp1 consists of 524 amino acids with a predicted secretory N-terminal signal sequence cleaved between amino acid positions 24 and 25 (Fig. 1). BLAST-based homology search revealed that Slp1 is a single-copy gene in sorghum and belongs to a family of proline-rich proteins with unknown function. The transcript of this protein is highly abundant in young leaves and inflorescences (MOROKOSHI, ©2018 RIKEN, query Sobic.001G265900, Makita *et al.*, 2015). Slp1 is rich in proline, lysine, and histidine, comprising 20%, 13%, and 11% of total amino acids, respectively. The theoretical pI value of the protein is 9.28. Structure predictions suggested that ~80% of the protein is a random coil and 14% is an α-helix, and that the tertiary structure is intrinsically disordered. Slp1 has seven repeats made of three motifs. The most conserved repeat unit (B-domain, Fig. 1) appears in all seven repeats, is rich in proline, lysine, and glutamic acid (P, K, E-rich domain), with a consensus sequence

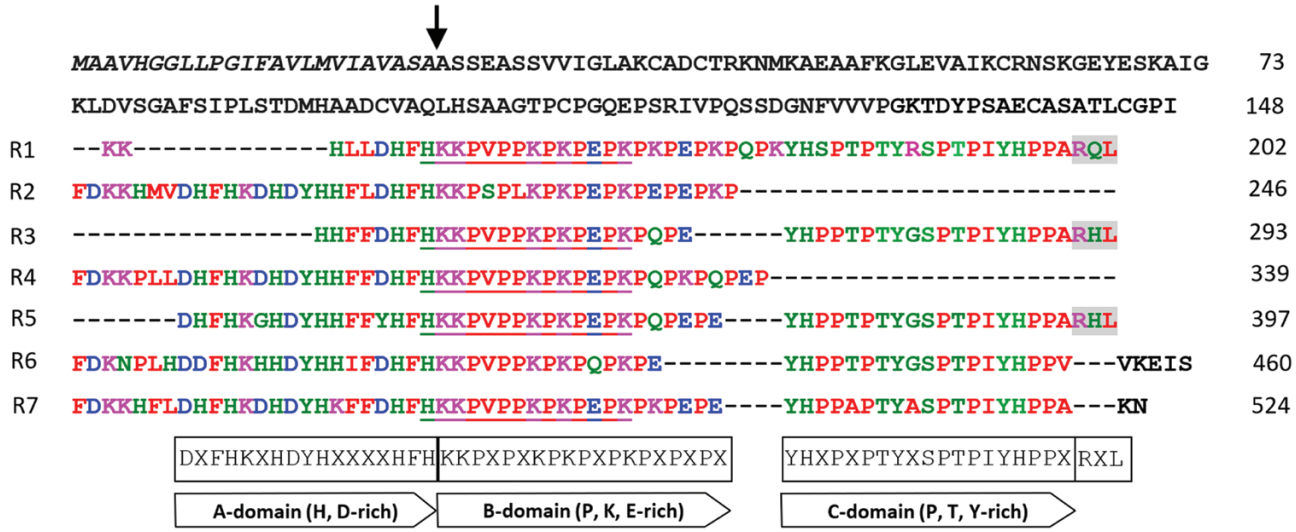

Fig. 1. Primary sequence of *Sorghum bicolor* Slp1, showing the N-terminal signal sequence and the seven repeats (R1–R7). The predicted signal sequence is shown in italics. The arrow denotes the predicted signal sequence cleavage site. All the repeats (R1–R7) have a proline-, lysine-, and glutamic acid-rich (P, K, E-rich) domain forming a zwitterionic centre (B-domain). In addition, a histidine–aspartic acid-rich (H, D-rich) domain, negatively charged near physiological pH, precedes the B-domain in repeats 2, 4, 5, 6, and 7 (A-domain). A proline-, threonine-, and tyrosine-rich (P, T, Y-rich) domain follows the B-domain in repeats 1, 3, 5, 6, and 7 (C-domain). At the end of repeats 1, 3, and 5, there is an RXL domain (shaded) which serves as the cleavage site for unknown proteases in many bio-silica-associated proteins in diatoms. The underlined sequence appearing five times in the primary sequence is Peptide-1 that was used for raising antibodies against Slp1. The consensus sequence for the domains is given in boxes below each domain, where X denotes any amino acid.

KKPXPXKPKPXPKPXPXPX. Five of the repeat units (R2, R4, R5, R6, and R7) have a histidine and aspartic acid- (H, D-) rich domain (A-domain), with the consensus sequence DXFHKXHDYHXXXXHFH, immediately preceding the B-domain. In five repeats (R1, R3, R5, R6, and R7) there is a third domain (C-domain), following the B-domain, rich in proline, threonine, and tyrosine (P, T, Y-rich) with the consensus sequence YHXPXPTYXSPTPIYHPPX. At physiological pH, the A-domain is negatively charged, whereas close to half of the B-domain is positively charged (lysine-rich) and the rest of the B-domain is negatively charged (glutamic acid-rich) forming a zwitterionic structure. The C-domain, rich in amino acids with an -OH group in their side chain, has available positions for H-bonds (with no charge). At the end of R1, R3, and R5, we found an RXL domain. This domain acts as recognition site for unknown proteases that cleave at the C-terminus of the leucine residue of the RXL domain in many bio-silica-associated proteins in diatoms (Kröger *et al.*, 1999; Wenzl *et al.*, 2008; Scheffel *et al.*, 2011; Kotzsch *et al.*, 2017). R1–R7 are thus made of the motifs: BC RXL AB BC RXL AB ABC RXL ABC ABC. Before the start of R1–R7 (amino acids 1–148), there is a region rich in alanine, serine, glycine, and valine (comprising together 45% of the region). Our analysis could not show sequence similarity of Slp1 to any protein known to be involved in bio-mineralization.

Silicic acid in vitro *precipitation by Slp1 sequences*

In order to test the possible activity of Slp1 as a silica mineralizer, we overexpressed it in *E. coli*. The purified protein fraction, which we assumed to contain Slp1, precipitated white particles within seconds. The resulting powder was oven dried and imaged by SEM-EDS, showing that the powder was made of Si and O (Supplementary Fig. S3). We could not collect precipitate in other protein fractions or in extractions of proteins from bacteria that were transformed with the same vector lacking the Slp1 sequence.

To study the conserved B-domain, we synthesized the peptide sequence HKKPVPPKPKPEPK (Peptide-1) appearing five times in Slp1. Silicic acid solution of 90.9 mM precipitated white powder within seconds after adding Peptide-1. In contrast, adding a mutant peptide, where the lysine residues were replaced by alanine (HAAPVPPAPAPEPA; Peptide-3), did not precipitate the powder. Gel-like material formed when the reaction mixture was centrifuged (Fig. 2A). SEM of the powder sediment revealed spheres of ~500 nm in diameter (Fig. 2B). Silica was also precipitated by Peptide-1 at a silicic acid concentration of 5 mM, which is in the lower physiological concentration range (Casey *et al.*, 2003). Particles produced under these conditions were ~250 nm in diameter (Fig. 2C). In control solutions, without peptide, at 90.9 mM and 5 mM silicic acid, precipitation was not detectable by SEM.

Raman and NMR spectroscopies suggest silica formation by Slp1 sequences

The precipitated powder at 90.9 mM silicic acid was characterized by Raman and magic angle spinning (MAS) solid-state NMR (ss-NMR) spectroscopies (Fig. 3). The Raman spectrum of the sediment forming with Peptide-1 (Fig. 3Ai) showed that the mineral is silica, recognized by the typical broad peaks at 488 cm^{-1} (Si–O–Si bonds) and 989 cm^{-1} (Si–OH bonds) (Aksan *et al.*, 2012). These two peaks are missing in the Raman spectrum of clean Peptide-1 (Fig. 3Aii). The amide bond peaks at 1667 cm^{-1} (amide I), 1450 cm^{-1} (amide II), and

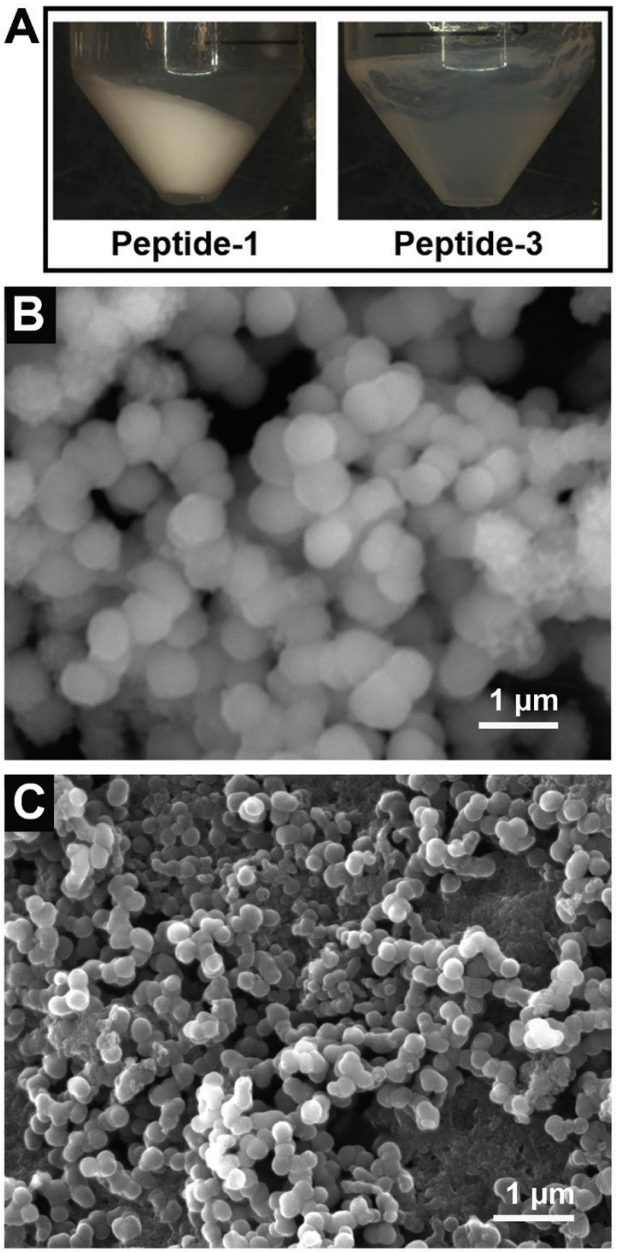

Fig. 2. Imaging of precipitates by peptides derived from *Sorghum bicolor* Slp1 sequence. (A) Sand-like powder sediment produced from metastable (90.9 mM) silicic acid solution with Peptide-1 (left), while a gel-like material formed after several rounds of centrifugation of silicic acid solution with Peptide-3 (right). (B) Scanning electron micrograph of the powder sediment formed by Peptide-1 at 90.9 mM silicic acid. (C) Scanning electron micrograph of the silica sediment formed by Peptide-1 at 5 mM silicic acid.

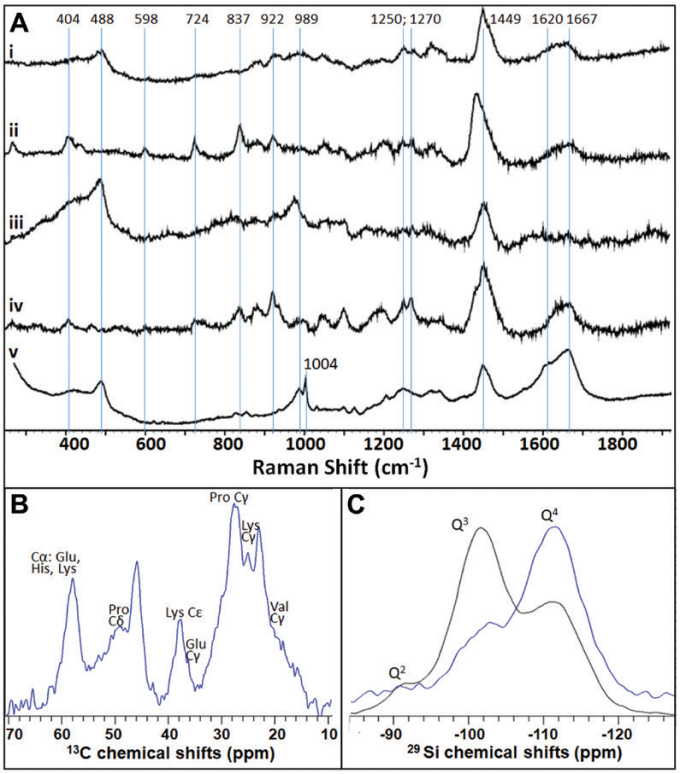

Fig. 3. Characterization of the peptide–silica precipitates using Raman and NMR spectroscopy. (A) Raman spectra of the sediment formed with Peptide-1 (i), clean Peptide-1 (ii), the sediment formed with Peptide-3 (iii), clean Peptide-3 (iv), and the sediment formed with Slp1 expressed in *E. coli* (v). Spectra i and v show peaks of silica at 488 and 989 cm^{-1}, and spectrum iii shows silica gel at 488 cm^{-1} and 978 cm^{-1}. Analysis suggests that the peptide is bound to the mineral through the lysine aliphatic amine and the C-terminal -COO^- group (see text for peak assignments). (B) NMR ^1H–^{13}C cross-polarization spectrum of the peptide–silica sediment. The signals, typical of aliphatic bonds in the amino acid side chain, are shifted to a high field by ~2 ppm. These shifts reflect a shielding effect of the silica, suggesting that the side chains are bound to the mineral. (C) Spectra of ^{29}Si showing peaks of Si-$(OSi)_2(OH)_2$ (Q2); Si-$(OSi)_3(OH)$ (Q3); and Si-$(OSi)_4$ (Q4). Direct polarization (blue line) samples all the Si atoms in the sample, while ^1H-cross-polarization (black line) samples Si atoms in proximity to protons.

1270 and 1250 cm^{-1} (amide III) appear in both spectra of silica–Peptide-1 and Peptide-1 alone (Fig. 3Ai, Aii). The broad peak at 1449 cm^{-1} in the Peptide-1 spectrum may represent both amide II and free -NH_3^+ on the lysine functional group (Aliaga *et al.*, 2009). The gel-like material which precipitated together with Peptide-3 (Fig. 2A) presented a pronounced broad Si–O–Si peak at 488 cm^{-1} (Fig. 3Aiii). The silanol Raman scattering was shifted to lower energies (978 cm^{-1}), typical of silica gel (Bertoluzza *et al.*, 1982). The peaks assigned to amide bonds were smaller in relation to the SiO_2 peaks, when compared with the spectrum of Peptide-1 precipitate. This suggests that a smaller fraction of Peptide-3 was included in the gel. Both spectra of Peptide-1 and Peptide-3 (Fig. 3Aii, iv) present a peak at 837 cm^{-1}, missing in the precipitated mineral (Fig. 3Ai, iii). This could be a C–C stretch in the proline ring (Stewart and Fredericks, 1999). Vibrations at 922, 724, and 598 cm^{-1}, assigned to groups of -COO^- at the peptide C-terminus (Stewart and Fredericks, 1999), are weaker in the mineral precipitate. We suggest that the carboxyl groups may interact with hydroxyl groups presented by the mineral. Silica was also precipitated by the full length of Slp1 lacking the signal peptide (Fig. 3Av). Raman spectra of the sediment included peaks of silica (at 488 cm^{-1} and 989 cm^{-1}) and protein (1250, 1270, 1449, and 1667 cm^{-1}). A typical scattering of phenylalanine at 1004 cm^{-1} was measured.

NMR ^1H–^{13}C cross-polarization measurements confirmed the Raman findings that the peptide was complexed with the silica (Fig. 3B). The spectrum shows narrow peaks [full width

at half maximum (FWHM) was 282 Hz], as compared with spectra of a diatom peptide complexed with silica (FWHM of 489 Hz; Geiger *et al*., 2016). The narrow peaks allowed us to identify many of the amino acid side chain carbons, with peaks shifted to a higher field by ~2 ppm. Such shifts are possibly caused by the silica shielding the magnetic field that is felt by the peptide and is indicative of the close proximity of the mineral to the peptide.

Direct polarization of ^{29}Si NMR measured the number of groups of -OSi and -OH bound to a central Si atom, defined as Qn [Si-$(OSi)_nOH_{4-n}$], Engelhardt and Michel, 1987). The relative intensities of the Q4:Q3:Q2 peaks in the spectrum were 62:33:5, indicating that there are about five bulk (Q4) Si atoms for every three surface (Q3+Q2) atoms (Fig. 3C). NMR ^{1}H–^{29}Si cross-polarization measurements could detect some Q4 siloxane species bound to surface oxygen in addition to surface Q3 and Q2 (Fig. 3C). These Si atoms were excited by protons from nearby silanols and water, indicating their closeness to the surface of the silica particle. Elaborate ss-NMR characterization and comparison with silica produced with a diatom silaffin peptide demonstrates the role of phosphates in the mineral–peptide interaction (Adiram-Filiba *et al*., 2020).

Slp1 expression pattern correlates with silica deposition in silica cells

Our sequence-based predictions and *in vitro* results suggested a role for Slp1 in silica deposition *in planta*. To investigate whether the Slp1 expression profiles correlate with silica deposition times and locations, we raised an antibody against Peptide-1. Using western blot, we detected several bands in immature leaf and immature inflorescence. Slp1 expression was not detected in roots and mature leaves (Fig. 4A). In leaf tissues, Slp1 runs at ~70 kDa, in contrast to the expected size of ~57 kDa. This may be because of possible post-translational modifications of Slp1. In immature inflorescence tissues, we detected a pattern of multiple, relatively regularly spaced bands. The bands suggest that Slp1 was either degraded spontaneously during extraction or cleaved biologically at relevant proteolytic cleavage locations, possibly the RXL sites.

In agreement with the protein expression profile, we detected RNA transcripts of *Slp1* in immature leaves and immature inflorescences, but not in mature leaves (Fig. 4B; Supplementary Fig. S4). This profile matches regions of active silica deposition in silica cells, occurring in young leaves but not in mature leaves. The RNA transcript profile along immature, silicifying leaf tissues showed that *Slp1* is strongly transcribed in the leaf base, reaching the highest levels just before the active silicification zone (ASZ–1). The transcription levels dropped by a factor of ~15 in the ASZ, and further reduced in older tissues of immature leaves (Fig. 4C). In the youngest mature leaf tissue, we found that *Slp1* is transcribed at a background level of ~1/19 000 that of the maximal transcript in ASZ–1.

Slp1 localization was tested by immunohistochemical staining with the antibody against Peptide-1. The antibody bound to silica cells in leaf epidermal cells at the ASZ (Fig. 5A, B), in either the cytoplasmic volume or near the cell periphery

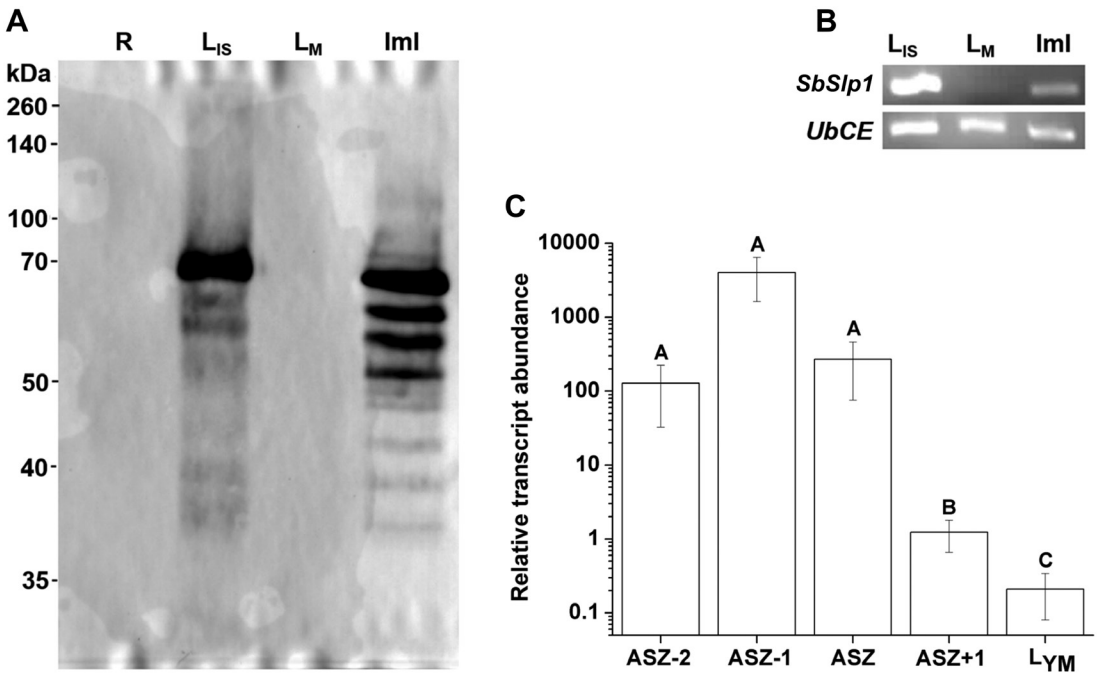

Fig. 4. Expression profile of *Sorghum bicolor* Slp1. (A) Western blot of crude protein extract from roots (R), immature silicifying leaf (L_{IS}), mature leaves (L_M), and immature inflorescence (Iml), detected by an antibody against Peptide-1. A similar amount of protein was loaded on each lane. Slp1 was expressed in developing leaves and inflorescences, but not in roots and mature leaves. Multiple sized bands indicate cleavage of the protein. This may suggest that Slp1 is processed differently in immature leaf and inflorescence. (B) RNA transcription of *Slp1* in immature silicifying leaf (L_{IS}), mature leaves (L_M), and immature inflorescences (Iml). In accordance with protein translation, transcription was detected only in the immature tissues. Ubiquitin-conjugating enzyme (*UbCE*) was used as internal control gene. See Supplementary Fig. S4 for the entire gel. (C) RNA transcript profile of *Slp1* along immature silicifying leaf tissues. Maximal transcript was found in ASZ–1, which lies just below the ASZ. Error bars indicate the SD (n=3).

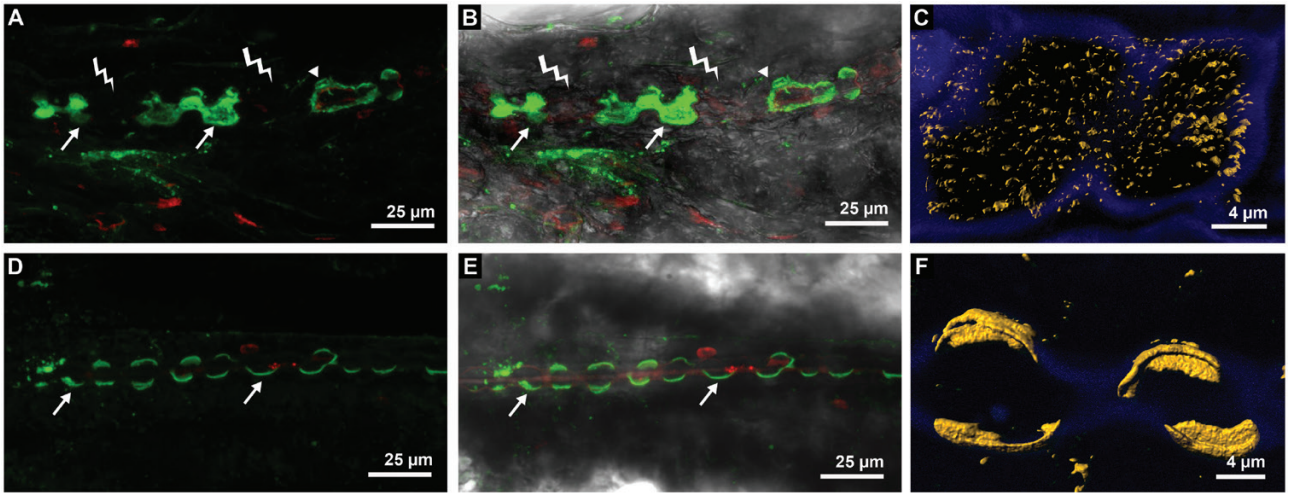

Fig. 5. Immunolocalization of *Sorghum bicolor* Slp1 in the active silicification zone (ASZ) of young leaves (A–C), and near the tips of mature leaves (D–F). In sorghum leaves, silica cells usually pair with cork cells (indicated by lightning signs) and exist as long chains of alternating silica and cork cells; however, near the leaf tip, cork cells are absent and silica cells fuse to form long polylobate bodies. (A) Immunolocalization (green fluorescence) shows that Slp1 is localized to silica cells of the sorghum leaf ASZ, inside the cytoplasm (arrows) or near the cell periphery (arrowhead). (B) Fluorescence image in (A) merged with the corresponding brightfield image. (C) The anti-Peptide-1 antibody fluorescence was processed to select for punctuated regions (pseudocolored yellow) in the ASZ. The Slp1 marker appears in packets in the cytoplasm and cell boundary. (D) The anti-Peptide-1 antibody (green fluorescence) binds to the edges of silicified silica cells (arrows) in mature leaves. (E) Fluorescence image in (D) merged with the corresponding brightfield image. (F) Processed fluorescence of a mature leaf image (pseudocoloured yellow) suggests that Slp1 is embedded uniformly inside condensed silica. Red fluorescence is from propidium iodide; blue is background autofluorescence of the cell walls.

(Supplementary Video S1). Image analysis suggested that the cytoplasmic immunofluorescence originated from aggregates or vesicles (Fig. 5C). In mature leaves, where silica cells are silicified and dead, the antibody hybridized only to the boundary of silica cells (Fig. 5D, E), suggesting that Slp1 was immobilized in the bio-silica. No aggregates were identified by image analysis (Fig. 5F). Control immunolocalization with the pre-immune serum or the reactions lacking any one or both the antibodies did not fluoresce (Supplementary Fig. S5).

The presence of an N-terminal signal peptide in Slp1 predicted it to be secretory in nature. To test this prediction, we made a translational fusion of GFP to the C-terminus of full-length Slp1 and transiently overexpressed it in tobacco. Similar to our observations in the sorghum silica cells at the ASZ, the tobacco cells expressing the fusion protein fluoresced in discrete packets (Fig. 6A, B). Some packets were identified as fusing to the cell membrane. In addition, we also observed diffused fluorescence at cell boundaries (Fig. 6C, D; Supplementary Video S2). The presence of a signal peptide and these results infer that the discrete packets are secretary vesicles filled with Slp1 molecules. Regretably, we were not able to demonstrate silica formation by Slp1 in tobacco, probably because only a small fraction of cells overexpressed the fusion protein (as inferred from GFP fluorescence) and tobacco apoplast is not rich in silicic acid (Coskun *et al.*, 2019*b*). In control tobacco plants that overexpressed GFP without Slp1, the fluorescence was uniform in the cytoplasm and nucleus, and lower between cells (Fig. 6E, F). Mock infiltration of tobacco leaves by MES buffer did not cause fluorescence. Thus, our results in sorghum and tobacco suggest that native Slp1 is localized in secretary compartments of the silica cells and released to the paramural space—the apoplast. Since the apoplast of grass leaves is supersaturated with silicic acid, secretion of the Slp1 may lead to immediate silica precipitation.

Functional characterization of Slp1 in sorghum

To elucidate the role of Slp1 *in vivo*, we transiently overexpressed it in sorghum, using a construct derived from MDMV. Compared with the wild-type plants, control sorghum plants infected with virus lacking the Slp1 sequence showed infection lesions and viral symptoms (Supplementary Fig. S6). We did not observe silica deposition in apparently healthy parts of the infected leaves of control plants (Fig. 7A–F). In contrast, the Slp1-overexpressing plants had ectopic silica deposition in healthy looking parts of the infected leaves as well as close to the veins and where viral symptoms were observed (Fig. 7G–I). Silica was also deposited in cells which are not usually silicified in sorghum leaves, such as guard cells, cork cells, and long cells (Fig. 7J–K). Back-scattered SEM of 10 biological replicates suggested the silicification intensity to be of a level similar to that in silica cells. In correlation, the locations of high Si also contained high concentrations of oxygen, but similar background levels of other elements.

Discussion

Out of several cell types that deposit silica in grasses, silica cells are unique, as >95% of them silicify in young, elongating leaves. Their mineralization requires metabolic activity and is independent of transpiration (Sangster and Parry, 1976). The fast precipitation of silica over a few hours (Lawton, 1980) in addition to the formation of the mineral at the cell wall, as opposed to the cytoplasm (Kumar *et al.*, 2017a; Kumar and Elbaum, 2018), point to a factor exported from the cells that

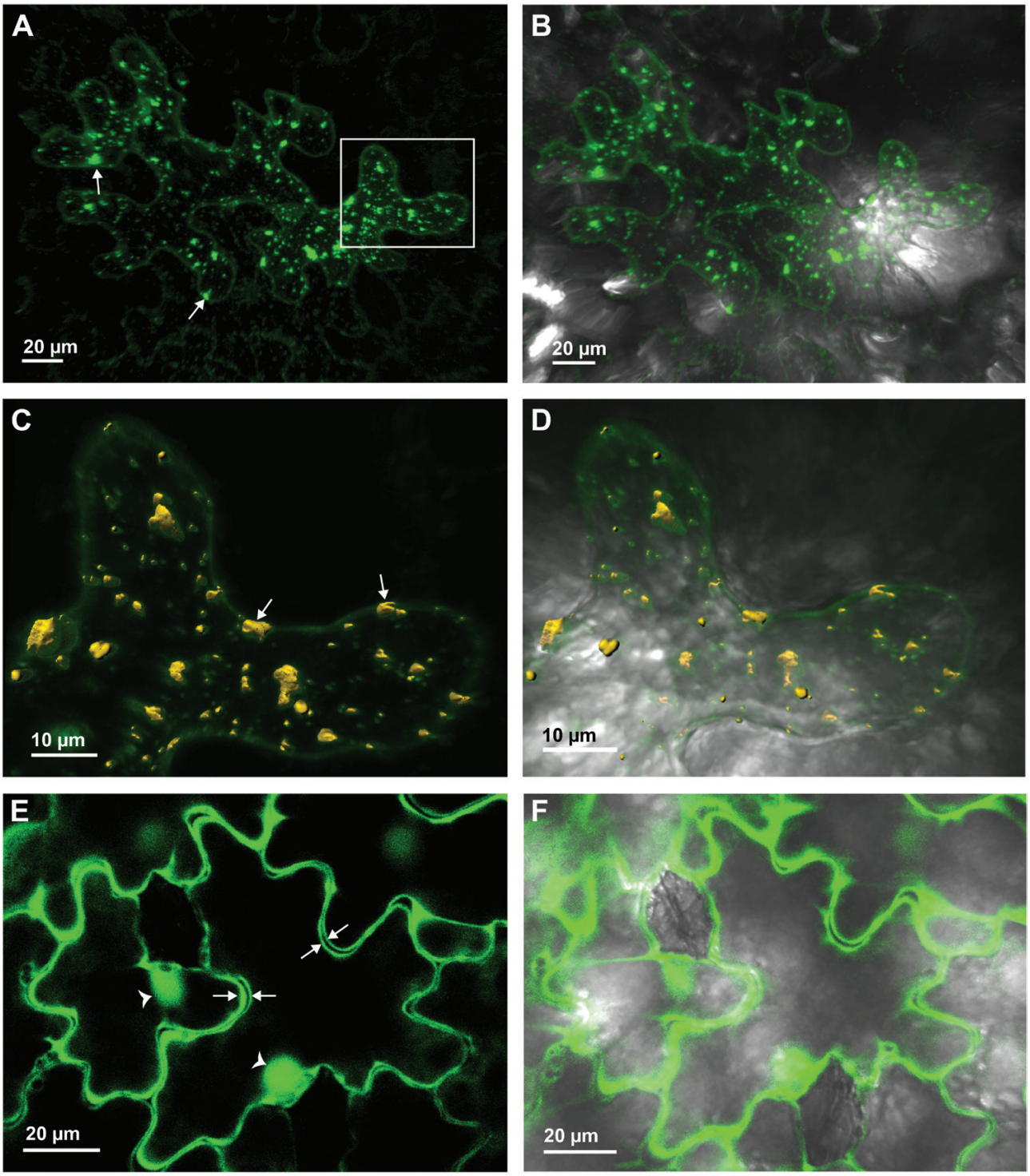

Fig. 6. Fluorescence confocal microscopy showing the secretory nature of *Sorghum bicolor* Slp1 transiently expressed in tobacco. (A) Slp1 fused with GFP was transiently overexpressed in tobacco leaf using *Agrobacterium tumefaciens*. The green fluorescence, marking the location of Slp1, was found in vesicles inside the cytoplasm (arrows), while diffused green fluorescence can also be seen along the margin of the cell. The white rectangle marks a region enlarged in (C). (B) Fluorescent image in (A) merged with the corresponding brightfield image. (C) Segmenting the green fluorescence to diffuse (green) and punctate (pseudocoloured yellow) regions shows vesicles fusing to the cell membrane (arrows) as well as diffused fluorescence at cell boundaries. (D) Fluorescent image in (C) merged with the corresponding brightfield image. (E) Control plants expressing GFP without Slp1 showing uniform green fluorescence of the cytoplasm and nuclei (arrowheads). Arrows indicate the cytoplasm of adjacent cells, demonstrating the low fluorescence between cells. (F) Fluorescent image in (E) merged with the corresponding brightfield image.

induces the formation of biogenic silica. Our work shows that silica cells express and export the protein Slp1 to the apoplast, timed with silicification in the paramural space (Kumar *et al*., 2017*a*; Kumar and Elbaum, 2018). It is obvious that silica deposition depends on the presence of silicic acid which is absorbed by roots from the soil. Typical silicic acid

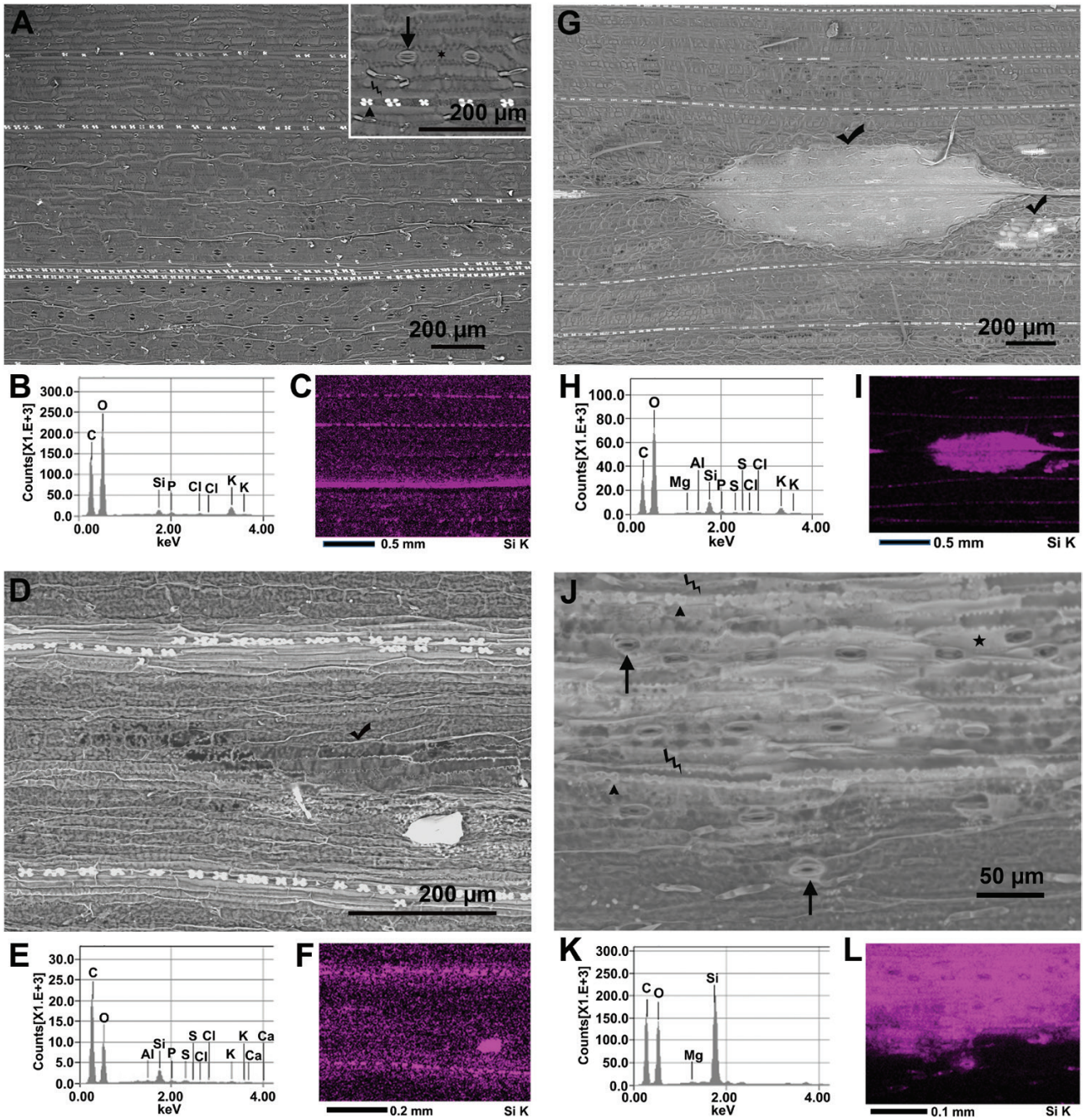

Fig. 7. Scanning electron micrographs in back-scattered electron (BSE) mode, and energy-dispersive X-ray spectroscopy (EDS) of sorghum seedlings transiently overexpressing Slp1. (A) SEM micrograph of a wild-type sorghum mature leaf showing the general silicification pattern in a mature leaf. Inset: epidermal cell types are indicated in a higher magnification image. (B) EDS spectrum for the image area in (A). (C) EDS map for Si signal of the image area in (A). (D) SEM image of control plants showing silicification only at usual locations. A dust particle with high Si content is seen on the bottom right. (E) EDS spectrum for the image area in (D). (F) EDS map for Si of the image area in (D). (G) SEM image of ectopic silica deposition in a viral lesion in an Slp1-overexpressing plant. (H) EDS spectrum for the image area in (G). (I) EDS map for Si of the image area in (G). (J) SEM image of Slp1-overexpressing plants showing high-intensity silica deposition in cells that do not usually silicify in wild-type plants. All epidermal cell types can be seen silicified. (K) EDS spectrum for the image area in (J). (L) EDS map for Si of the image area in (J). Arrowheads, silica cells; arrows, stomata; lightning signs, cork cells; stars, long cells; and tick marks, viral lesions.

concentrations measured in the xylem sap are 5–7.5 mM for wheat (Casey *et al.*, 2003) and 5–25 mM for rice (Ma *et al.*, 2002; Mitani and Ma, 2005). We measured 4 mM and 7–12 mM in root pressure exudates of sorghum seedlings and mature plants, respectively (unpublished data). Since *Slp1* overexpression caused deposition in all epidermis cell types (Fig. 7), we can conclude that it actively precipitates silica at *in vivo* silicic acid concentrations. Furthermore, the fact that the silica formed ectopically in stomata and long cells indicates that Slp1 is sufficient to cause precipitation in those cells. Based on our results we conclude that Slp1 in its native form actively deposits silica *in vivo*.

Similar to silica-depositing proteins in diatoms, Slp1 may need post-translational modification for its optimum activity

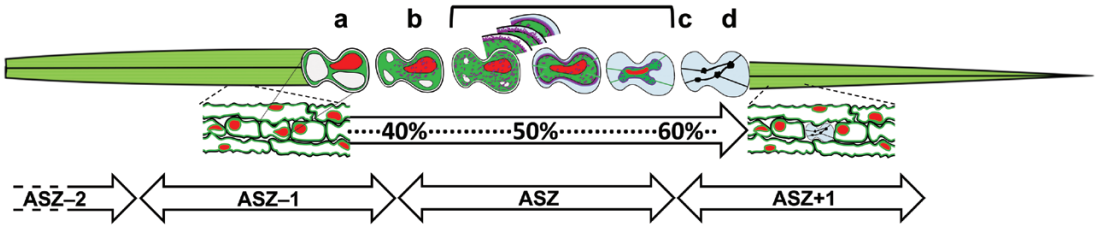

Fig. 8. Model suggested for silica cells mineralization along the developmental gradient of a sorghum leaf. From left to right, silica cells differentiate and elongate, reaching their final morphology between 30% and 40% of the length of the developing leaf (a). (b) By the end of ASZ–1 (40% of the leaf length), the large vacuoles (white) shrink in volume and translation of Slp1 is initiated (purple). (c) As soon as a cell enters the ASZ, the cell starts actively translating and accumulating Slp1 in the cytoplasm. When the silica cell is ready for silicification, Slp1 is exported to the apoplastic space. There, silicic acid at supersaturation starts to polymerize to silica (grey). The thickening cell wall reduces the cytoplasmic space (green), and the shape of the nucleus (red) is sometimes deformed. The viable cytoplasm of the silicifying silica cell is connected to the cytoplasm of neighbouring cells by plasmodesmata (indicated by a narrow green channel extending to the cell wall). (d) The cell finally undergoes programmed cell death, marking an end to the silicification process and leaving voids in the space that was occupied by the dying cytoplasm. These voids open to the surface, probably reminiscent of the plasmodesmata. The process from meristematic cell division to death of the silica cell is completed within ~10 h. The one-sided arrow represents the maturity state of the developing leaf and the two-sided arrows represent the different silicification zones.

in vivo (Hildebrand *et al.*, 2018). This is suggested by features in its primary sequence (Fig. 1) and relatively slower migration during gel electrophoresis (Fig. 4). More indications for Slp1 post-translational modifications may arise from the time gap between its highest transcription level in the ASZ–1 tissue, and the highest silicification activity in the ASZ (Kumar *et al.*, 2017*a*; Kumar and Elbaum, 2018). Modifications may be tissue specific, and further research is needed to test these hypotheses.

Slp1 expression was not detected in roots where silica cells do not form (Fig. 4). Furthermore, we could not detect Slp1 expression in mature leaf tissues, consistent with the absence of viable, active silica cells (Kumar and Elbaum, 2018). This suggests that Slp1 precipitates silica in silica cells, while silica deposition in cell walls and possibly other locations is governed by other means such as specific cell wall polymers (Fry *et al.*, 2008; Law and Exley, 2011; Kido *et al.*, 2015; Brugiére and Exley, 2017; Kulich *et al.*, 2018). Our report on Slp1 expression in immature inflorescence is consistent with published transcriptomic data, showing *Slp1* transcripts both before and after inflorescence emergence (table S5 in Davidson *et al.*, 2012). We propose that some cell types in the inflorescence employ Slp1 to polymerize silicic acid to silica independently of transpiration intensity (Hodson *et al.*, 1984; Hodson, 2016; Kumar *et al.*, 2017*b*). To reach its final destination, silicic acid needs the transpiration stream. This explains the fact that the first silica cells to silicify are those adjacent to the large longitudinal veins (Kumar *et al.*, 2017*a*), suggesting too that the volume of xylem sap reaching the cells may be the main bottleneck for silica deposition.

Binding of anti-Peptide-1 antibody in the boundary of dead silica cells of mature leaves suggests that as Slp1 is the template for the silica precipitation, it is caught inside the silica structure. Silicanin-1, a biosilica-associated protein from *Thalassiosira pseudonana*, is embedded inside biosilica structures and is accessible to anti-silicanin-1 antibody (Kotzsch *et al.*, 2017). Similarly, anti-Peptide-1 antibody may also have access to the epitope remains on the surface of the deposited silica in silica cells. Our *in vitro* experiments support such entrapment, with significant shifts in the NMR and Raman peaks (Fig. 3), indicating close proximity between the peptide and the mineral. The native plant silica may form a permeable protein–silica structure that will allow movement of solutes. Specifically, as silica forms in the apoplast adjacent to the cell membrane (Kumar and Elbaum, 2018), diffusion of silicic acid through the mineral is required in order for silica cells to fully silicify. The diffusion model is also supported by a larger ratio of surface to bulk Si atoms in silica cells, probably originating from multiple nucleation sites for the mineralization process (Zancajo *et al.*, 2019).

Conclusions

Overexpression and localization studies of Slp1 show that this protein is involved in silicification in sorghum leaf silica cells. Slp1 has unique amino acid composition, charge distribution, and probably post-translational modifications, necessary for its activity. We propose a model for silica deposition in sorghum silica cells, based on the activity of Slp1 (Fig. 8). After cell division, as soon as a cell starts differentiating into a silica cell, it starts its preparation for silicification. Slp1 is transcribed, translated, possibly post-translationally modified, packed in vesicles, and stored in the cytoplasm until the cell is ready for silicification. The vesicles sequentially start fusing to the cell membrane. Slp1 release in the apoplastic space results in its contact with supersaturated silicic acid solution, leading to immediate silica precipitation. Diffusion of more silicic acid from the apoplastic space feeds the process that results in reduction in the cytoplasmic volume of silica cells constricted by the growing siliceous cell wall. Finally, the cell undergoes programmed cell death, putting an end to the silicification process (Kumar and Elbaum, 2018). The rapid formation of the mineral explains the difficulty associated with finding silicification in an intermediate state. The expression pattern, localization, and modifications of Slp1 in the inflorescence bracts need to be studied in detail.

Supplementary data

Supplementary data are available at *JXB* online.

Fig. S1. Transcript level of *RRM* in relation to *UbCE* as the reference gene, showing that the transcript levels of the two housekeeping genes do not change significantly in the tested tissues.

Fig. S2. Alignment of nucleotide sequences of the wheat (*Triticum aestivum*) locus identifier Ta#S18008495 and sorghum (*Sorghum bicolor*) Slp1 (Sb01g025970).

Fig. S3. SEM of the powder produced by adding Slp1 to a 90.9 mM silicic acid solution.

Fig. S4. Relative quantification of *Slp1* transcription in varied plant organs.

Fig. S5. Immunolocalization control reactions using pre-immune serum; or lacking either one or both of the antibodies.

Fig. S6. *Maize dwarf mosaic virus*- (MDMV) infected sorghum plants showing symptoms.

Table S1. List of candidate silica-depositing genes in wheat and their sorghum homologues.

Table S2. List of primers used in the present study.

Video S1. Confocal microscopy video clip showing Slp1 localization in the cytoplasmic space and near the cell boundary of silica cells.

Video S2. Confocal microscopy video clip showing Slp1 containing vesicles fusing to the cell membrane. Slp1 fused to GFP was transiently overexpressed in tobacco leaves. Image stacks were segmented using the program Imaris. Identified vesicles were pseudocoloured red, that can be seen fusing to the cell membrane. The Slp1–GFP fluorescence in the cell margin is also visible in the video.

Acknowledgements

The authors thank Shmuel Wolf for the pBIN-GFP plasmid, Vincent Otieno Ayieko for precipitating and characterizing the silica produced with Slp1, and Nerya Zexer and Victor M. Rodriguez Zancajo for measuring silicic acid concentration in sorghum sap.

Funding

SK was the recipient of a post-doctoral fellowship from Planning and Budgeting Committee (PBC), Council for Higher Education, Israel. This research was funded by the Israel Science Foundation grant 534/14 and ISF-ICORE grant 757/12. Partial support to the Centre for Scientific Imaging, Hebrew University (Rehovot campus) by a grant from United States Agency for International Development (AID-ASHA-G 1400005) to the American Friends of the Hebrew University and The Robert H Smith Faculty of Agriculture, Food and Environment is gratefully acknowledged.

Author contributions

SK and RE planned and designed the research; SK identified Slp1 from the list of putative silicification-related proteins and performed most of the experiments; NA-F performed the NMR spectroscopy and analysed the data with GG; SB performed parts of the experiments; SK and JAS-L performed immunolocalization experiment under the supervision of YH; OT analysed the microarray data and prepared the list of Si-responsive genes in sorghum; AO prepared the MDMV construct under the supervision of HV; SK and RE analysed the results and wrote the paper. All the authors commented on and approved the final version of the manuscript for publication.

Data availability

The nucleotide sequence of *Sorghum bicolor* Slp1 has been submitted to NCBI with the GenBank accession number MH558953. The GenBank accession number of the pBIN19 plasmid is U09365.1. The MDMV-GUS plasmid that we used in the current study is covered by a published patent number WO2016125143 (https://patentscope.wipo.int/search/en/detail.jsf?docId=WO2016125143).

References

Adiram-Filiba N, Geiger Y, Kumar S, Keinan-Adamsky K, Elbaum R, Goobes G. 2020. Peptides from diatoms and grasses harness phosphate ion binding to silica to help regulate biomaterial structure. Acta Biomaterialia (in press).

Aksan A, Hubel A, Reategui E. 2012. Silica-based composite ocular device and methods. US Patent number WO201109719A2.

Alexandre A, Basile-Doelsch I, Delhaye T, Borshneck D, Mazur JC, Reyerson P, Santos GM. 2015. New highlights of phytolith structure and occluded carbon location: 3-D X-ray microscopy and NanoSIMS results. Biogeosciences **12**, 863–873.

Aliaga AE, Osorio-Roman I, Garrido C, Leyton P, Cárcamo J, Clavijo E, Gómez-Jeria JS, Fleming GD, Campos-Vallette MM. 2009. Surface enhanced Raman scattering study of L-lysine. Vibrational Spectroscopy **50**, 131–135.

Bertoluzza A, Fagnano C, Antonietta Morelli M, Gottardi V, Guglielmi M. 1982. Raman and infrared spectra on silica gel evolving toward glass. Journal of Non-Crystalline Solids **48**, 117–128.

Brugiére T, Exley C. 2017. Callose-associated silica deposition in *Arabidopsis*. Journal of Trace Elements in Medicine and Biology **39**, 86–90.

Bustin SA, Benes V, Garson JA, *et al*. 2009. The MIQE guidelines: minimum information for publication of quantitative real-time PCR experiments. Clinical Chemistry **55**, 611–622.

Casey WH, Kinrade SD, Knight CTG, Rains DW, Epstein E. 2003. Aqueous silicate complexes in wheat, *Triticum aestivum* L. Plant, Cell & Environment **27**, 51–54.

Chain F, Côté-Beaulieu C, Belzile F, Menzies JG, Bélanger RR. 2009. A comprehensive transcriptomic analysis of the effect of silicon on wheat plants under control and pathogen stress conditions. Molecular Plant-Microbe Interactions **22**, 1323–1330.

Combet C, Blanchet C, Geourjon C, Deléage G. 2000. NPS@: network protein sequence analysis. Trends in Biochemical Sciences **25**, 147–150.

Coskun D, Deshmukh R, Sonah H, Menzies JG, Reynolds O, Ma JF, Kronzucker HJ, Bélanger RR. 2019*a*. The controversies of silicon's role in plant biology. New Phytologist **221**, 67–85.

Coskun D, Deshmukh R, Sonah H, Shivaraj SM, Frenette-Cotton R, Tremblay L, Isenring P, Bélanger RR. 2019*b*. Si permeability of a deficient Lsi1 aquaporin in tobacco can be enhanced through a conserved residue substitution. Plant Direct **3**, e00163.

Davidson RM, Gowda M, Moghe G, Lin H, Vaillancourt B, Shiu SH, Jiang N, Robin Buell C. 2012. Comparative transcriptomics of three Poaceae species reveals patterns of gene expression evolution. The Plant Journal **71**, 492–502.

Dosztányi Z, Csizmok V, Tompa P, Simon I. 2005*a*. IUPred: web server for the prediction of intrinsically unstructured regions of proteins based on estimated energy content. Bioinformatics **21**, 3433–3434.

Dosztányi Z, Csizmók V, Tompa P, Simon I. 2005*b*. The pairwise energy content estimated from amino acid composition discriminates between folded and intrinsically unstructured proteins. Journal of Molecular Biology **347**, 827–839.

Emanuelsson O, Nielsen H, Brunak S, von Heijne G. 2000. Predicting subcellular localization of proteins based on their N-terminal amino acid sequence. Journal of Molecular Biology **300**, 1005–1016.

Engelhardt G, Michel D. 1987. High resolution solid state NMR of silicates and zeolites. Chichester: John Wiley & Sons.

Epstein E. 1994. The anomaly of silicon in plant biology. Proceedings of the National Academy of Sciences, USA **91**, 11–17.

Fry SC, Nesselrode BH, Miller JG, Mewburn BR. 2008. Mixed-linkage (1→3,1→4)-β-D-glucan is a major hemicellulose of *Equisetum* (horsetail) cell walls. New Phytologist **179**, 104–115.

Geiger Y, Gottlieb HE, Akbey Ü, Oschkinat H, Goobes G. 2016. Studying the conformation of a silaffin-derived pentalysine peptide embedded in bioinspired silica using solution and dynamic nuclear polarization

magic-angle spinning NMR. Journal of the American Chemical Society **138**, 5561–5567.

Hildebrand M, Lerch SJL, Shrestha RP. 2018. Understanding diatom cell wall silicification—moving forward. Frontiers in Marine Science **5**, 125.

Hodson MJ. 2016. The development of phytoliths in plants and its influence on their chemistry and isotopic composition. Implications for palaeoecology and archaeology. Journal of Archaeological Science **68**, 62–69.

Hodson MJ, Sangster AG, Parry DW. 1984. An ultrastructural study on the development of silicified tissues in the lemma of *Phalaris canariensis* L. Proceedings of the Royal Society B; Biological Sciences **222**, 413–425.

Hodson MJ, Sangster AG, Parry DW. 1985. An ultrastructural study on the developmental phases and silicification of the glumes of *Phalaris canariensis* L. Annals of Botany **55**, 649–665.

Hodson MJ, White PJ, Mead A, Broadley MR. 2005. Phylogenetic variation in the silicon composition of plants. Annals of Botany **96**, 1027–1046.

Jose-Estanyol M. 2013. Maize embryo transient transformation by particle bombardment. Bio-Protocol **3**, e865.

Kaleda A, Haleva L, Sarusi G, Pinsky T, Mangiagalli M, Bar Dolev M, Lotti M, Nardini M, Braslavsky I. 2019. Saturn-shaped ice burst pattern and fast basal binding of an ice-binding protein from an Antarctic Bacterial consortium. Langmuir **35**, 7337–7346.

Kaufmian PB, Bigelow WC, Petering LB, Drogosz FB. 1969. Silica in developing epidermal cells of *Avena* internodes: electron microprobe analysis. Science **166**, 1015–1017.

Kaufman PB, Dayanandan P, Franklin CI. 1985. Structure and function of silica bodies in the epidermal system of grass shoots. Annals of Botany **55**, 487–507.

Kauss H, Seehaus K, Franke R, Gilbert S, Dietrich RA, Kröger N. 2003. Silica deposition by a strongly cationic proline-rich protein from systemically resistant cucumber plants. The Plant Journal **33**, 87–95.

Kido N, Yokoyama R, Yamamoto T, Furukawa J, Iwai H, Satoh S, Nishitani K. 2015. The matrix polysaccharide (1;3,1;4)-2-β-glucan is involved in silicon-dependent strengthening of rice cell wall. Plant & Cell Physiology **56**, 268–276.

Kotzsch A, Gröger P, Pawolski D, Bomans PHH, Sommerdijk NAJM, Schlierf M, Kröger N. 2017. Silicanin-1 is a conserved diatom membrane protein involved in silica biomineralization. BMC Biology **15**, 65.

Kröger N, Deutzmann R, Sumper M. 1999. Polycationic peptides from diatom biosilica that direct silica nanosphere formation. Science **286**, 1129–1132.

Kulich I, Vojtíková Z, Sabol P, Ortmannová J, Neděla V, Tihlaříková E, Žárský V. 2018. Exocyst subunit EXO70H4 has a specific role in callose synthase secretion and silica accumulation. Plant Physiology **176**, 2040–2051.

Kumar S, Elbaum R. 2017. Estimation of silica cell silicification level in grass leaves using *in situ* charring method. Bio-Protocol **7**, e2607.

Kumar S, Elbaum R. 2018. Interplay between silica deposition and viability during the life span of sorghum silica cells. New Phytologist **217**, 1137–1145.

Kumar S, Milstein Y, Brami Y, Elbaum M, Elbaum R. 2017*a*. Mechanism of silica deposition in sorghum silica cells. New Phytologist **213**, 791–798.

Kumar S, Soukup M, Elbaum R. 2017*b*. Silicification in grasses: variation between different cell types. Frontiers in Plant Science **8**, 438.

Law C, Exley C. 2011. New insight into silica deposition in horsetail (*Equisetum arvense*). BMC Plant Biology **11**, 112.

Lawton JR. 1980. Observations on the structure of epidermal cells, particularly the cork and silica cells, from the flowering stem internode of *Lolium temulentum* L. (Gramineae). Botanical Journal of the Linnean Society **80**, 161–177.

Li X. 2011. Infiltration of *Nicotiana benthamiana* protocol for transient expression via *Agrobacterium*. Bio-Protocol **1**, e95.

Ma JF, Tamai K, Ichii M, Wu GF. 2002. A rice mutant defective in Si uptake. Plant Physiology **130**, 2111–2117.

Ma JF, Tamai K, Yamaji N, Mitani N, Konishi S, Katsuhara M, Ishiguro M, Murata Y, Yano M. 2006. A silicon transporter in rice. Nature **440**, 688–691.

Ma JF, Yamaji N, Mitani N, Tamai K, Konishi S, Fujiwara T, Katsuhara M, Yano M. 2007. An efflux transporter of silicon in rice. Nature **448**, 209–212.

Makita Y, Shimada S, Kawashima M, Kondou-Kuriyama T, Toyoda T, Matsui M. 2015. MOROKOSHI: transcriptome database in *Sorghum bicolor*. Plant & Cell Physiology **56**, e6.

Markovich O, Kumar S, Cohen D, Addadi S, Fridman E, Elbaum R. 2019. Silicification in leaves of sorghum mutant with low silicon accumulation. Silicon **11**, 2385–2391.

Massiot D, Fayon F, Capron M, King I, Le Calvé S, Alonso B, Durand J-O, Bujoli B, Gan Z, Hoatson G. 2002. Modelling one- and two-dimensional solid-state NMR spectra. Magnetic Resonance in Chemistry **40**, 70–76.

McLarnon E, McQueen-Mason S, Lenk I, Hartley SE. 2017. Evidence for active uptake and deposition of Si-based defenses in tall fescue. Frontiers in Plant Science **8**, 1199.

Mitani N, Ma JF. 2005. Uptake system of silicon in different plant species. Journal of Experimental Botany **56**, 1255–1261.

Motomura H, Fujii T, Suzuki M. 2000. Distribution of silicified cells in the leaf blades of *Pleioblastus chino* (Franchet et Savatier) Makino (Bambusoideae). Annals of Botany **85**, 751–757.

Perry CC. 2003. Silicification: the processes by which organisms capture and mineralize silica. Reviews in Mineralogy and Geochemistry **54**, 291–327.

Perry CC, Mann S, Williams RJP. 1984. Structural and analytical studies of the silicified macrohairs from the lemma of the grass *Phalaris canariensis* L. Proceedings of the Royal Society B: Biological Sciences **222**, 427–438.

Petersen TN, Brunak S, von Heijne G, Nielsen H. 2011. SignalP 4.0: discriminating signal peptides from transmembrane regions. Nature Methods **8**, 785–786.

Pfaffl MW. 2001. A new mathematical model for relative quantification in real-time RT–PCR. Nucleic Acids Research **29**, e45.

Poulsen N, Kröger N. 2004. Silica morphogenesis by alternative processing of silaffins in the diatom *Thalassiosira pseudonana*. Journal of Biological Chemistry **279**, 42993–42999.

Sakurai G, Satake A, Yamaji N, Mitani-Ueno N, Yokozawa M, Feugier FG, Ma JF. 2015. In silico simulation modeling reveals the importance of the Casparian strip for efficient silicon uptake in rice roots. Plant & Cell Physiology **56**, 631–639.

Sangster AG, Parry DW. 1976. The ultrastructure and electron-probe microassay of silicon deposits in the endodermis of the seminal roots of *Sorghum bicolor* (L.) Moench. Annals of Botany **40**, 447–459.

Scheffel A, Poulsen N, Shian S, Kröger N. 2011. Nanopatterned protein microrings from a diatom that direct silica morphogenesis. Proceedings of the National Academy of Sciences, USA **108**, 3175–3180.

Shakoor N, Nair R, Crasta O, Morris G, Feltus A, Kresovich S. 2014. A *Sorghum bicolor* expression atlas reveals dynamic genotype-specific expression profiles for vegetative tissues of grain, sweet and bioenergy sorghums. BMC Plant Biology **14**, 35.

Shimizu K, Amano T, Bari MR, Weaver JC, Arima J, Mori N. 2015. Glassin, a histidine-rich protein from the siliceous skeletal system of the marine sponge *Euplectella*, directs silica polycondensation. Proceedings of the National Academy of Sciences, USA **112**, 11449–11454.

Shimizu K, Cha J, Stucky GD, Morse DE. 1998. Silicatein α: cathepsin L-like protein in sponge biosilica. Proceedings of the National Academy of Sciences, USA **95**, 6234–6238.

Skinner RH, Nelson CJ. 1995. Elongation of the grass leaf and its relationship to the phyllochron. Crop Science **35**, 4–10.

Soukup M, Martinka M, Bosnic D, Caplovicová M, Elbaum R, Lux A. 2017. Formation of silica aggregates in sorghum root endodermis is predetermined by cell wall architecture and development. Annals of Botany **120**, 739–753.

Soukup M, Rodriguez Zancajo VM, Kneipp J, Elbaum R. 2020. Formation of root silica aggregates in sorghum is an active process of the endodermis. Journal of Experimental Botany **71**, 6807–6817.

Stewart S, Fredericks PM. 1999. Surface-enhanced Raman spectroscopy of amino acids adsorbed on an electrochemically prepared silver surface. Spectrochimica Acta Part A **55**, 1641–1660.

Talukdar P, Hartley SE, Travis AJ, Price AH, Norton GJ. 2019. Genotypic differences in shoot silicon concentration and the impact on grain arsenic concentration in rice. Journal of Plant Nutrition and Soil Science **182**, 265–276.

Tzfadia O, Diels T, De Meyer S, Vandepoele K, Aharoni A, Van de Peer Y. 2015. CoExpNetViz: comparative co-expression networks construction and visualization tool. Frontiers in Plant Science **6**, 1194.

Wenzl S, Hett R, Richthammer P, Sumper M. 2008. Silacidins: highly acidic phosphopeptides from diatom shells assist in silica precipitation in vitro. Angewandte Chemie **47**, 1729–1732.

Yamaji N, Mitatni N, Ma JF. 2008. A transporter regulating silicon distribution in rice shoots. The Plant Cell **20**, 1381–1389.

Yoshida S, Ohnishi Y, Kitagishi K. 1962. Chemical forms, mobility and deposition of silicon in rice plant. Soil Science and Plant Nutrition **8**, 15–21.

Zancajo VMR, Diehn S, Filiba N, Goobes G, Kneipp J, Elbaum R. 2019. Spectroscopic discrimination of sorghum silica phytoliths. Frontiers in Plant Science **10**, 1571.

Zexer N, Elbaum R. 2020. Unique lignin modifications pattern the nucleation of silica in sorghum endodermis. Journal of Experimental Botany **71**, 6818–6829.

Zhang C, Wang L, Zhang W, Zhang F. 2013. Do lignification and silicification of the cell wall precede silicon deposition in the silica cell of the rice (*Oryza sativa* L.) leaf epidermis? Plant and Soil **372**, 137–149.